CrystEngComm

ROYAL SOCIETY OF CHEMISTRY

PAPER

View Article Online
View Journal | View Issue

Cite this: *CrystEngComm*, 2023, **25**, 1486

Tuning the topology of a 2D metal–organic framework from 2D to 3D using modulator assisted synthesis†

Johannes Hungwe,[a] Piwai Tshuma,[a] Maureen Gumbo,[a] Francoise M. Amombo Noa,[b] Lars Öhrström [b] and Gift Mehlana *[a]

Received 12th January 2023,
Accepted 9th February 2023

DOI: 10.1039/d3ce00039g

rsc.li/crystengcomm

Two new metal–organic frameworks based on 2,2′-bipyridine-4,4′-dicarboxylate and La(III) ions were prepared under solvothermal conditions. $[La(bpda)_{3/2}(dmf)_2]\cdot dmf\cdot H_2O$, MSU-10, was isolated as a 2D network structure. By introducing a modulator, 1,10-phenanthroline, the 3D network $[La(bpda)_{3/2}(dmf)(H_2O)_2]\cdot dmf$ MSU-11 could be isolated with the unusual rod-MOF topology **zbj**. Both the 2D and 3D networks are stable upon guest removal and the activated phases of MSU-10 and MSU-11 exhibit some phase change when soaked in solvents for 24 h. Network analysis allowed the identification of MSU-11 as isoreticular with MOF-80 built from different linkers and metal ions.

Introduction

Metal–organic frameworks are a new class of materials that can exhibit important porous properties giving rise to such applications as gas separation, catalysis, and storage.[1,2] MOFs assembled from lanthanoid metal ions[3,4] are important as the high charge and coordination number of Ln(III) metal ions may give the resulting MOFs high chemical and thermal stability which could make them suitable in catalysis and as photoluminescent probes.[5,6] The majority of lanthanoid MOFs have solvent molecules which are coordinated to their metal secondary building units (SBUs) to give coordination numbers ranging from six to twelve. Removal of these solvent molecules by application of heat and vacuum gives rise to open metal sites which can be exploited in heterogeneous catalysis and gas adsorption.[7,8] The high coordination number on the other hand may induce rod-SBUs and rod-MOFs,[9] which in turn may give more stable MOFs.[10] Rod-shaped SBUs also do not cause interpenetration (catenation),[11] and may give the framework breathing properties.[10,12–14]

Just like other MOFs, the synthesis of lanthanoid-based MOFs is affected by changes in temperature, pH, concentration of the reactants, solvents, and the presence of modulators.[15] This implies that several MOFs can be isolated using the same molecular building blocks.[16] These modulators may compete with the organic linker for the coordination sites and slows down the rate of crystal growth. This technique has been applied in some instance to obtain large crystals for single crystal X-ray diffraction. Examples of some of the modulators which have been reported in literature are acetic acid, benzoic acid, dodecanoic acid or lauric acid.[17] In some instances modulators have been shown to increase porosity and to control the morphology of the crystals.[18] The modulators may also be incorporated into the metal-SBU, and then affect the coordination number of the metal.

The SBUs can be simplified as geometric figures that comprise of metal clusters connected through non-metal bonds, such as the oxo (M–O–M) and carboxylate (M–O–C–O–M). These metal-SBUs then form recurrent 3D structures with the corresponding organic SBU.[19,20] The concept of SBUs was initially applied to zeolites where the TO_4 tetrahedra (primary building units) formed periodically recurring frameworks.[21] Different types of metal SBUs have been observed in MOFs, enabling a classification into dot-MOFs, rod-MOFs, sheet-MOFs and MOFs with 3D metal SBUs as most ZIFs.[10]

As part of our ongoing work to design new MOFs which can be used as support materials in catalysis,[22,23] herein, we report on the synthesis and characterization of two novel metal–organic frameworks based on lanthanum(III) and the 2,2′-bipyridine-4,4′-dicarboxylate linker.

Experimental section

Materials and methods

Lanthanum nitrate hexahydrate ($La(NO_3)_3\cdot 6H_2O$), 2,2′-bipyridine-4,4′-dicarboxylic acid (H_2bpda), 1,10-phenanthroline, *N*,*N*-dimethyl formamide (dmf), methanol (MeOH), ethanol (EtOH) and acetone were all purchased from

[a] *Midlands State University, Department of Chemical Sciences, 9055 Senga Road, Gweru, Zimbabwe. E-mail: mehlanag@staff.msu.ac.zw*
[b] *Chalmers University of Technology, Department of Chemistry and Chemical Engineering, Physical Chemistry Room 9029, Göteborg, Sweden*

† CCDC 2156057 and 2156058. For crystallographic data in CIF or other electronic format see DOI: https://doi.org/10.1039/d3ce00039g

Sigma-Aldrich and used without further purification unless otherwise mentioned.

Synthesis of $[La(bpda)_{3/2}(dmf)_2]\cdot dmf\cdot H_2O$ (MSU-10)

A mixture of H_2bpda (24.13 mg, 0.1 mmol) and 10 mL DMF was preheated. To the clear solution, $La(NO_3)_3\cdot 6H_2O$ (129.90 mg, 0.3 mmol) was added. The reaction mixture was placed in a sealed glass vial and heated in an oven at 110 °C for 72 hours. The mixture was cooled to room temperature and colourless crystals were obtained.

Synthesis of $[La(bpda)_{3/2}(dmf)(H_2O)_2]\cdot dmf$ (MSU-11)

About 24 mg (0.1 mmol) of H_2bpda was predissolved in 10 mL dmf followed by addition of $La(NO_3)_3\cdot 6H_2O$ (130 mg, −0.3 mmol) and 1,10-phenathroline (11.73 mg, 0.05 mmol). The resulting solution was sealed in a glass vial and heated at 110 °C for 72 hours to yield colourless crystals. A dried sample gave the elemental analysis corresponding to $[La(bpda)_{3/2}(dmf)_{0.5}]$ $C_{19.5}H_{12.5}LaN_{3.5}O_{6.5}$ % calculated: C, 43.47 H, 2.34 N, 9.10% experimental: C, 42.77 H, 2.48 N, 9.55.

Crystallographic data collection and refinement

Single crystal XRD data collection for MSU-10 was recorded on a Bruker KAPPA APEX II DUO diffractometer equipped with a graphite monochromated Mo-Kα radiation (λ = 0.71073 Å). Unit cell refinement and data reduction were performed using SAINT program.[24] Data were corrected for Lorentz-polarization and absorption effects using the multi-scan method (SADABS). For MSU-11, data collection was done on a Rigaku XtaLAB Synergy-DW diffractometer equipped with a HyPix-Arc 150° detector using Mo-Kα radiation (λ = 0.71073 Å). The data diffraction was acquired and processed with CrysAlisPro software package.[25]

The structure solutions were achieved by direct methods (program SHELXS) and refined anisotropically by full-matrix least-squares on F^2 using SHELXL[26] within the X-SEED[27] interface. The non-hydrogen atoms were located in the difference electron density maps and were refined anisotropically while all the hydrogen atoms were placed with geometric constraints and refined with isotropic temperature factors. The crystal data and refinement parameters are detailed in Table 1. The structures were deposited at the Cambridge Crystallographic Data Centre and allocated the number CCDC numbers 2156057 and 2156058 for MSU-10 and MSU-11 respectively.

Powder X-ray diffraction (PXRD)

Powder diffraction measurements were performed on a Bruker D2 Phaser 2nd Gen diffractometer using Cu Kα-radiation (λ = 1.54184 Å) at 298 K. The samples were placed on a zero-background sample holder and scanned over 2θ range 4 to 60° with a step of 0.60° increments. X-rays were generated with a current flow of 10 mA and voltage of 30 kV.

Table 1 Crystal data and refinement parameters for MSU-10 and MSU-11

	MSU-10	MSU-11
Empirical formula	$C_{27}H_{32}N_6O_{10}La_1$	$C_{24}H_{27}N_5O_{10}La_1$
Formula weight (g mol^{-1})	739.49	684.41
Temperature/K	173.11(2)	100(2)
Crystal system	Triclinic	Triclinic
Space group	$P\bar{1}$	$P\bar{1}$
a/Å	10.7028(7)	10.059(2)
b/Å	11.9890(8)	11.1837(4)
c/Å	13.1876(9)	13.6668(3)
α/°	89.083(2)	68.670(2)
β/°	72.765(2)	86.130(2)
γ/°	75.181(2)	74.590(2)
Volume/Å^3	1559.16	1379.94(7)
Z	2	2
Calculated density (g cm^{-3})	1.5749	1.6460
μ(Mo-Kα)/mm^{-1}	1.429	12.51
F(000)	726	686
Crystal size/mm^3	0.020 × 0.120 × 0.300	0.047 × 0.038 × 0.027
Radiation	MoKα (λ = 0.71073)	MoKα (λ = 0.71073)
2θ max/°	56.70	55.24
Index ranges	$-14 \le h \le 14$, $-15 \le k \le 16$, $-17 \le l \le 17$	$-12 \le h \le 12$, $-13 \le k \le 9$, $-17 \le l \le 16$
Reflections collected	38 690	43 550
No. unique data	7750	5614
The goodness of fit on S	1.053	1.073
Final R indexes [$I \ge 2\sigma(I)$]	0.0310	0.0305
Final wR_2 indexes [all data]	0.0695	0.0745
Largest diff. peak/hole/e Å^{-3}	0.84/−0.75	0.99/−0.72

The resultant experimental PXRD patterns recorded were plotted using Excel.

Whole powder pattern decomposition for MSU-10

Experimental powder X-ray diffraction data for MSU-10 data was used for profile fitting. The lattice parameters from single crystal data of MSU-10 was used for Pawley fitting and they were allowed to refine. Peak profile fitting was done using PV-TCHZ pseudo-Voight function included in the peak picking routine in TOPAS.[28] Profile fitting was performed over a 2θ range of 8.9–50°. The unit cell parameters were validated by the Pawley fitting method[29] by profile matching using the *hkl*-phase refinement in TOPAS. The background was modelled using the fifth order Chebyshev function and a parameter was included to account for sample displacement caused by the zero background sample holder.

Topological analysis

Network topology of the MOFs was obtained using the free software programs SYSTRE,[30] TOPOS[31] and checked against the Reticular Chemistry Structural Resource (RCSR).[32]

Thermogravimetric analysis

Thermogravimetric analysis (TGA) was performed using a TA Discovery Instrument TA-Q50 with a heating rate of 10 °C min^{-1} within a temperature range of 25–600 °C under a dry nitrogen purge gas flow of 50 mL min^{-1}.

Fourier transform infrared spectroscopy

Fourier Transform Infrared Spectroscopy (FITR) spectra of the samples were recorded in the range 400 to 4000 cm^{-1} on Nicolet 6700 Thermo-Scientific Fourier Transform Infrared spectrophotometer.

Gas sorption studies

MSU-10 and MSU-11 samples were dried in an oven at 523 K for 24 hours. The samples were degassed before the adsorption tests by heating at 623 K with a heating rate of 1 K min^{-1} under vacuum (5×10^{-3} mmHg) for 5 h. Using a static volumetric apparatus, CO_2 adsorption isotherms were determined at 293 K (Model-ASAP-2020, Micromeritics). Water from a water bath with a consistent temperature was circulated to maintain the adsorption temperature at 293 K and 750 mmHg. The adsorption capacity defined as the volume of gas adsorbed per gram of adsorbent-was determined.

Results and discussion

Synthesis

Both $[La(bpda)_{3/2}(dmf)_2]\cdot dmf\cdot H_2O$ MSU-10 and $[La(bpda)_{3/2}(dmf)(H_2O)_2]\cdot dmf$, MSU-11, were obtained by heating in dmf at 110 °C for 72 hours. However, the addition of 0.5 molar equivalents of 1,10-phenanthroline (based on bpda) to the reaction changes the outcome from a 2D network to a 3D network. While we cannot say with certainty what causes this effect, it could be reasonable to think that chelation of La(III) by the phenanthroline slows the reaction down, either by blocking sites in a growing polymer or by reducing the concentration of reactive La(III).

Structures

Single crystal X-ray diffraction analysis revealed that MSU-10 crystallises in the triclinic crystal system and space group $P\bar{1}$. The asymmetric unit consists of one crystallographically independent La(III) ion, one and half fully deprotonated linker, two coordinated and one uncoordinated dmf molecules. Furthermore, one uncoordinated water molecule was also modelled in the asymmetric unit. As illustrated in Fig. 1a, each La(III) is coordinated to two dmfs and seven oxygen atoms of the bpda linker to furnish a square antiprismatic geometry. Two bpda linkers are coordinated to the metal centre in a bidentate chelating mode and the other three in a bidentate bridging mode. MSU-10 is made up of $La_2C_6O_{12}$ secondary building unit (SBU) which grows along *b*-axis (Fig. 1b). The SBUs are connected by the bpda linker which propagates along the *b*–*c* axis to give a two-dimensional structure. The La–O bond length ranges from 2.465(4) to 2.807(4) Å. Analysis of bond angles around the lanthanum centre shows that there are within the range of

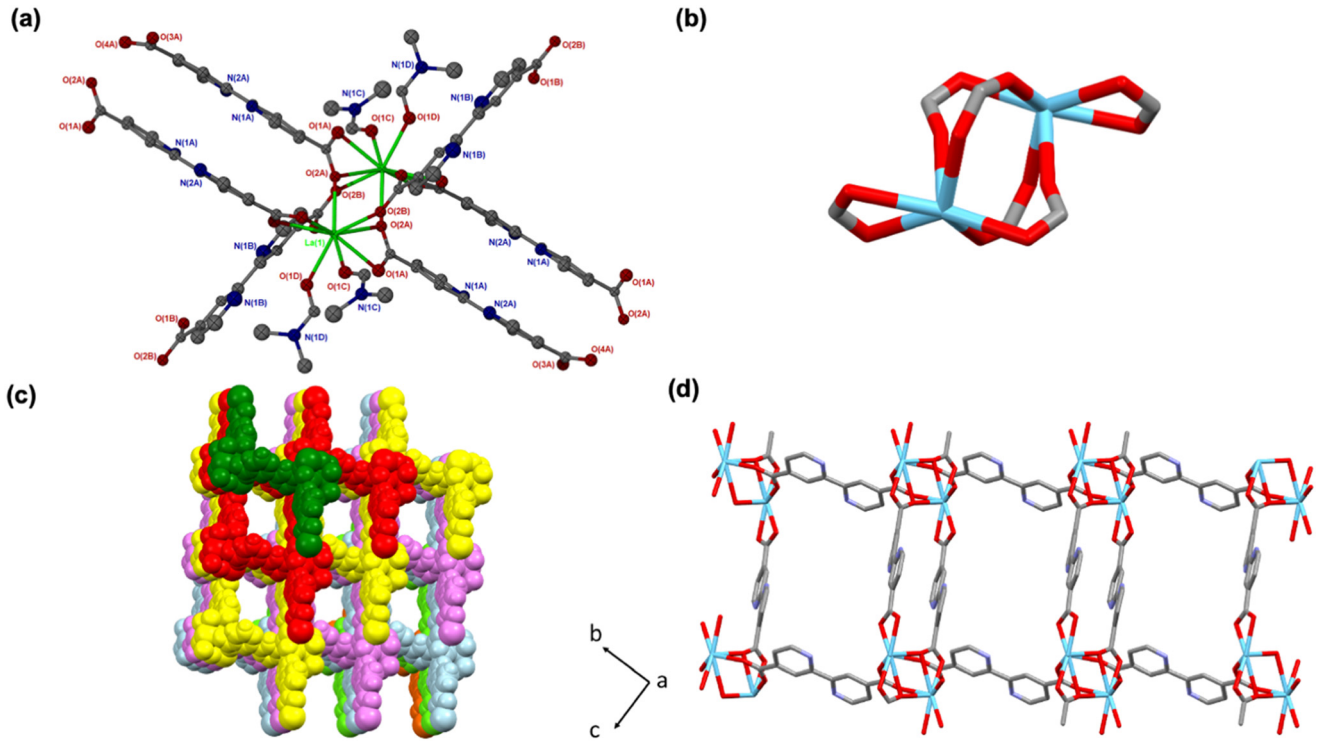

Fig. 1 a) Coordination environment around La(III) in MSU-10, drawn with ellipsoids at 50% probability. b) SBU generated *in situ* c) packing diagram of MOF-10 showing interdigitated 2D layers, d) packing diagram of MOF-10 showing double and single linkers to the SBU.

47.90(12)° to 154.46(14)°.

The packing diagram of MSU-10 is depicted in Fig. 1c and shows 2D interdigitated layers. The overall structure is 2D, with the frameworks having solvent filled rectangular channels running along the *a*-axis (Fig. 1d). These channels are occupied by coordinated dmf, water and uncoordinated solvent molecules. The analysis of interactions between the guest and framework shows that there are no noticeable interactions between the two. However, the structure is stabilised by weak intermolecular hydrogen bonding between the 2D layers and π···π interactions of the aromatic rings. In the absence of solvent molecules, PLATON[33] estimates the solvent-accessible void volume to be 51.2% using a probe radius of 1.2 Å.

MSU-11 crystallises in the triclinic crystal system and space group $P\bar{1}$. In the asymmetric unit, we modelled one La(III) metal centre, one and half deprotonated bpda linker, two coordinated water molecules, one coordinated dmf molecule and one uncoordinated dmf molecule. The lanthanum metal centre is bound to five bpda linkers, one dmf molecule and two water molecules. The carboxylate moiety assumes a both bidentate and monodentate bridging mode. The La–O bond length around the lanthanum ranges from 2.430(2) to 2.604(2) Å. La(III) metal centre assumes a square antiprismatic geometry (Fig. 2a) with bond angles ranging from 67.90(9)° to 147.80(8)°. The structure of MSU-11 is made up of a $La_2C_3O_5$ rod-SBU which grows along the *a*-axis as illustrated in Fig. 2b. The SBUs are linked by the bpda linkers which propagate along the *a*–*c* planes to give a three-dimensional network. Note that one set of linkers comes in pairs (the N1A/N1B set seen in Fig. 2a).

Analysis of the channels found in MSU-11 in the absence of coordinated and uncoordinated guest molecules account for (Fig. 2c and d) 43% of the unit cell volume as estimated in PLATON.[31]

Topological studies of MSU-11

To have a better understanding of MSU-11, a network deconstruction was carried out. Usually the straight rod approach[9] where the linkers are just attached to the rod, and the nodes are taken as the attachment points, give simple high symmetry nets. However, in the case of MSU-11 this is complicated by the two parallel linkers attaching to the same point (shown in red in Fig. 3a). We consider the simplest approach is to treat these as one link, the red linkers are π-stacked with centroid–centroid distances of 3.73 Å so there is not really any space between them, and we then get the **cds**-net as shown in Fig. 3b. The **cds**-net is one of the two most symmetric ways to construct a 3D-net from square planar nodes, the other is the **nbo**-net. The **cds**-net is also one of the folding nets[34] in principle enabling breathing and flexibility without changing the node geometry.

However, the straight rod approach does not account for the metal-SBU, the latter is just reduced to a rod. Therefore the points-of-extension approach has been introduced[9] which also adds the topology of the rod giving for MSU-11 a 5-, 6-, and 6-connected three nodal **zbj**-net where the rods are composed

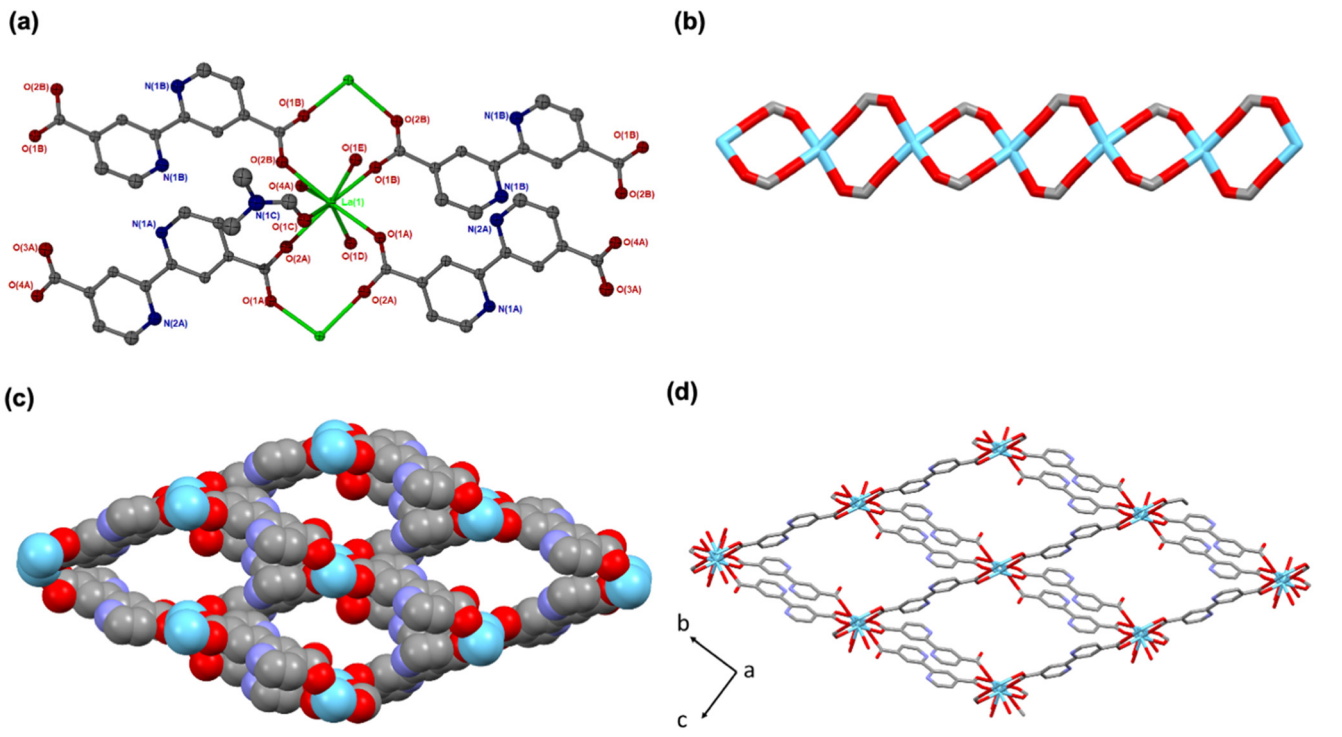

Fig. 2 (a) Coordination environment around La(III) in MSU-11, (b) SBU rod generated *in situ* (c) and (d) packing diagram of MOF-11 as viewed along the *a*-axis showing the channels drawn using van der Waals radii and stick form respectively.

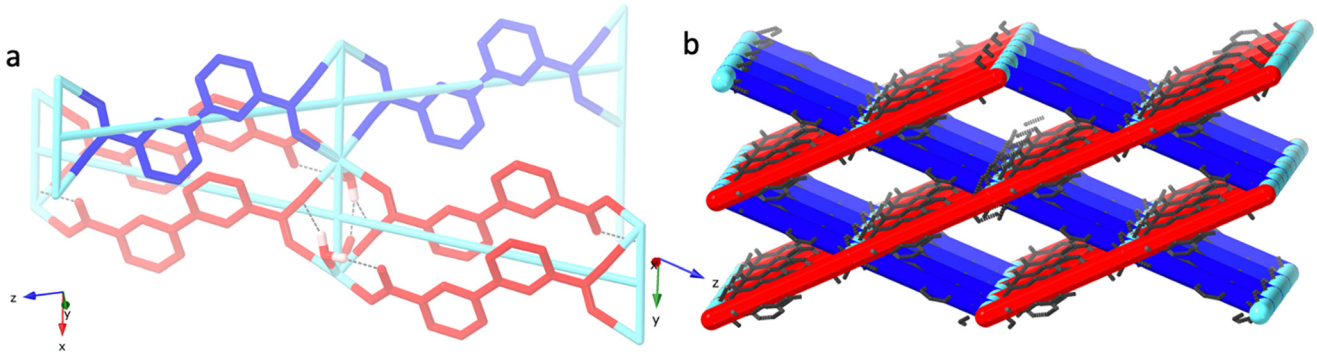

Fig. 3 (a) The double connection in MSU-11 and (b) the **cds**-net in MSU-11 obtained by the straight-rod approach and treating the double connection as one link.

of edge sharing quadratic pyramids (Fig. 4). There seems to be only one prior report of a **zbj**-net and that is for MOF-80 (ref. 11) with Tb and 2,7-pyrenedicarboxylic acid, $[Tb(pdc)_{1.5}(dmf)(H_2O)_2] \approx \cdot(dmf)$, earlier reported as "rod-net 7".[9]

The isoreticular MOF-80 and MSU-11 structures are in fact very close even though unit cell parameters, linker size and geometry differ (*i.e.* MSU-11 has volume 1380 Å^3 and MOF-80 1530 Å^3) but they have, for example, the same kind of π-stacked double linker connections between the rod-SBUs. This highlights the power of network analysis in finding structurally similar materials in a way that is impossible using unit cells and space groups.[35]

Thermogravimetric analysis

The TGA of MSU-10 in Fig. 5a exhibits a total weight loss of 31.5% between 25 and 325 °C, which corresponds to the loss of three dmf molecules and one water molecule (calculated 32%) modelled in the asymmetric unit. Framework decomposition occurs around 450 °C. Complete removal of the solvent molecules during activation was confirmed by TGA curve of the activated phase of MSU-10 which showed no weight loss until decomposition.

The thermal behaviour of MSU-11 illustrated in Fig. 5b exhibits a two stage of weight loss before decomposition. An initial weight loss of 15.3% (calculated 15.94%), between 50 and 125 °C, corresponds to the loss of one uncoordinated dmf molecule and two coordinated water molecules. The second weight loss of 10.61% (calculated 10.68%), between 225 and 310 °C, is attributed to the loss of 1 coordinated dmf molecule. Decomposition of the framework occurs around 450 °C. The activated phase of MSU-11 shows an initial 4% weight loss attributable to moisture adsorption. Although the two MOFs exhibit different networks, they have similar decomposition temperatures.

Powder X-ray diffraction

Phase purity of the bulk of the material was confirmed by PXRD studies. Fig. 6 shows the PXRD patterns of MSU-10 and MSU-11, diffraction patterns of as-synthesised compounds do not perfectly match the simulated patterns from single crystal

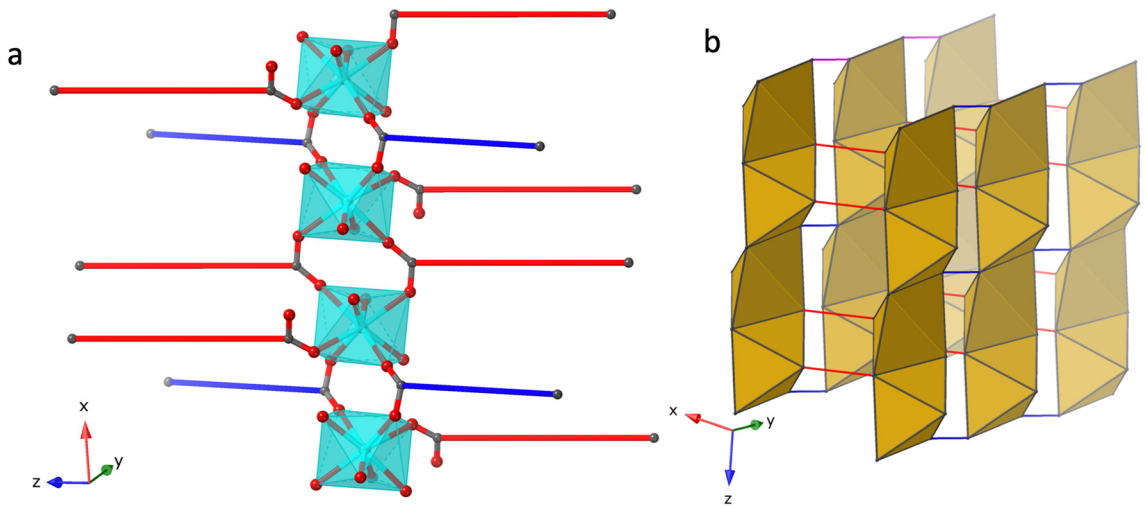

Fig. 4 a) The rod in MSU-11 is made from the coordination entities show in turquoise and the net from the two different connections in red and blue. Each linker is now treated individually. b) The ideal form of the resulting 5c, 6c, 6c three nodal **zbj**-net with edge sharing square pyramids. Same color coding for the linkers as in a.

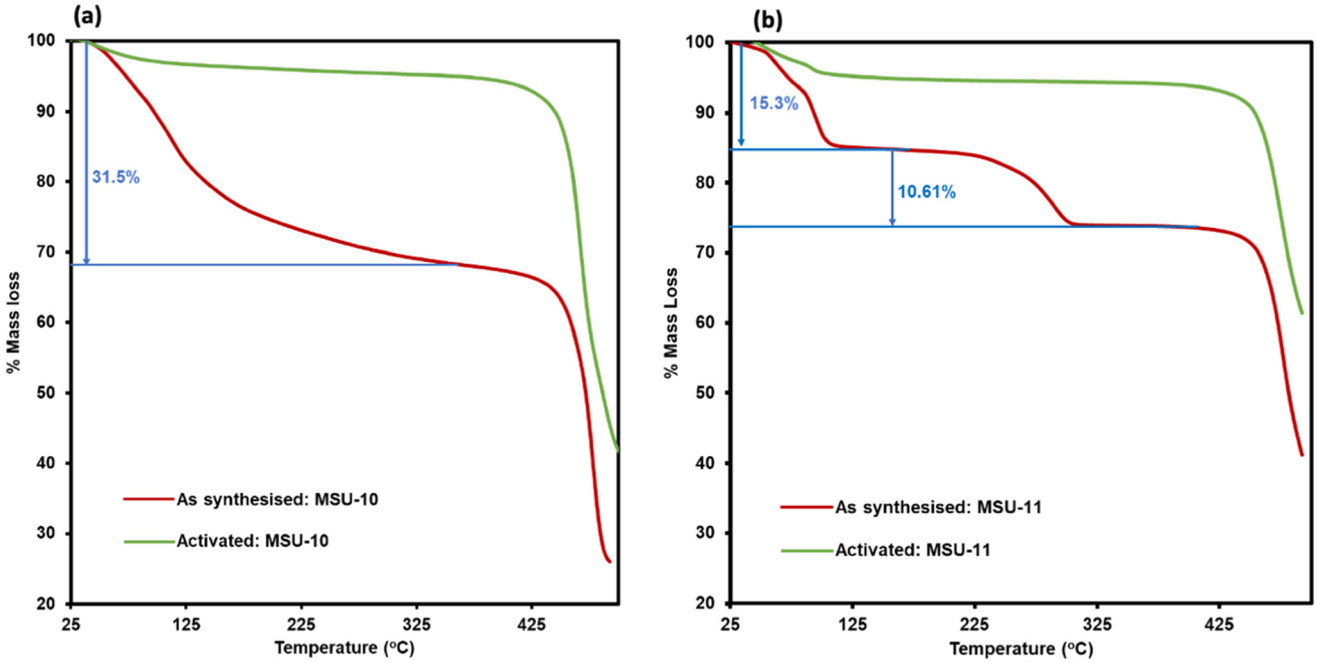

Fig. 5 Thermal analysis of a) MSU-10 and b) MSU-11 and their corresponding activated phases.

data. For MSU-10, the calculated diffractogram contains two peaks at low 2θ values that are absent in the experimental one. Similar observation were made by Maurin *et al.* and attributed the mismatch in PXRD patterns to the breathing effect of the MOF upon partial solvent loss during sample handling.[36] To have a better understanding of how the unit cell parameters of MSU-10 changes, we carried out whole powder pattern decomposition on the experimental data (Table S1†). Fig. S1† shows the PXRD of MSU-10, the pattern in blue is the experimental while in red is the calculated one. The difference is depicted in grey. There is a good match between the calculated and the experimental pattern from 8.9° to 50° 2θ positions. Upon removal of guest dmf and water molecules, the structural integrity of MSU-10 is

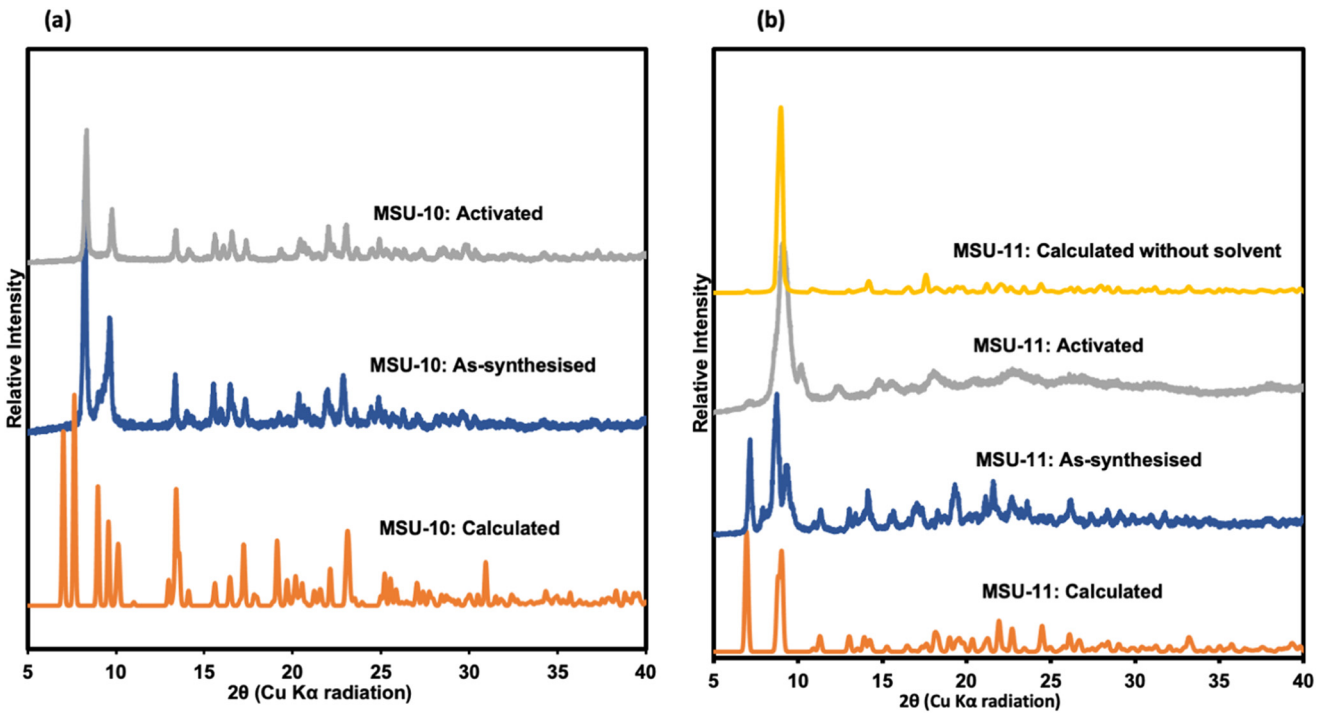

Fig. 6 (a) PXRD patterns of (a) MSU-10 and (b) MSU-11.

maintained as evidenced by an excellent agreement between the experimental and activated phases. The activated framework for MSU-11 (Fig. 6b) has some peaks at lower 2 theta disappearing. The observed disappearance of the peaks could have been easily interpreted as a crystalline to crystalline transformation upon activation. Such transformation is unlikely to happen with lanthanide based MOFs because of their high coordination number. Having this in mind, we removed the solvent molecules in our single crystal data and calculated the resultant the PXRD pattern. Surprisingly, as shown in Fig. 6b, there was a good agreement between the activated phase and the calculated PXRD pattern. This confirmed that the observed change in the PXRD pattern is not due to a transformation but was caused by the absence of the solvent molecules.

FTIR

FTIR were carried out to corroborate single crystal data and to confirm successful activation of the two MOFs. Fig. 7a suggests that the band at 1708 cm^{-1} (COOH) in the linker shifts to 1581 cm^{-1} in both MSU-10 and MSU-11. This is evidence that the carboxylate moiety is coordinated to the La(III) centre. These results are consistent with single crystal X-ray data. Successful activation is evidenced by the disappearance of the FTIR band at 1658 and 1643 cm^{-1} in MSU-10 and MSU-11 respectively assigned to the carbonyl stretch of dmf molecules. In MSU-10, the band at 1550 cm^{-1} is attributed to the C–C of the benzene ring. The bands at 1535 and 1388 cm^{-1} are assigned to the asymmetric and symmetric stretches of the carboxylate group respectively, with a magnitude of separation of 147 cm^{-1}, suggesting that the carboxylate moiety is coordinated to two La(III) ions in a bidentate bridging mode.[37] This position does not change after activation suggesting that the binding mode of the carboxylate moiety is retained. The full IR spectra for MSU-10 and 11 is presented in Fig. S2.† A broad band between 3100 and 3640 in MSU-10 is attributed to the presence of uncoordinated water molecules. This broad band is absent in MSU-11 as the water molecules are attached to the metal centre.

In MSU-11, Fig. 7b, the bands at 1543 and 1396 cm^{-1} are assigned to the asymmetric and symmetric stretches of the carboxylate group respectively, with a magnitude of separation of 147 cm^{-1}. Upon activation, the FTIR analysis suggests that the integrity of carboxylate moiety is not altered.[37]

Chemical stability tests

The activated phases of MSU-10 and MSU-11a were soaked in different organic solvents for 36 hours, the solids were recovered by filtration, washed thoroughly before recording PXRD patterns. The PXRD of MSU-10 recovered samples are illustrated in Fig. 8a. Although the peaks in the 2θ range of 7 and 11 are maintained for the sample soaked in ethanol, methanol and THF, new peaks beyond this range suggest formation of new phases. In water, the crystallinity of the MOF is affected as evidenced by a decrease in the peak intensity. Furthermore, a new phase is formed. For MSU-11, amorphization is observed for samples soaked in methanol, ethanol and THF. Just like MSU-10, which undergo a crystalline to crystalline transformation upon soaking in water, MSU-11 exhibited the same behaviour.

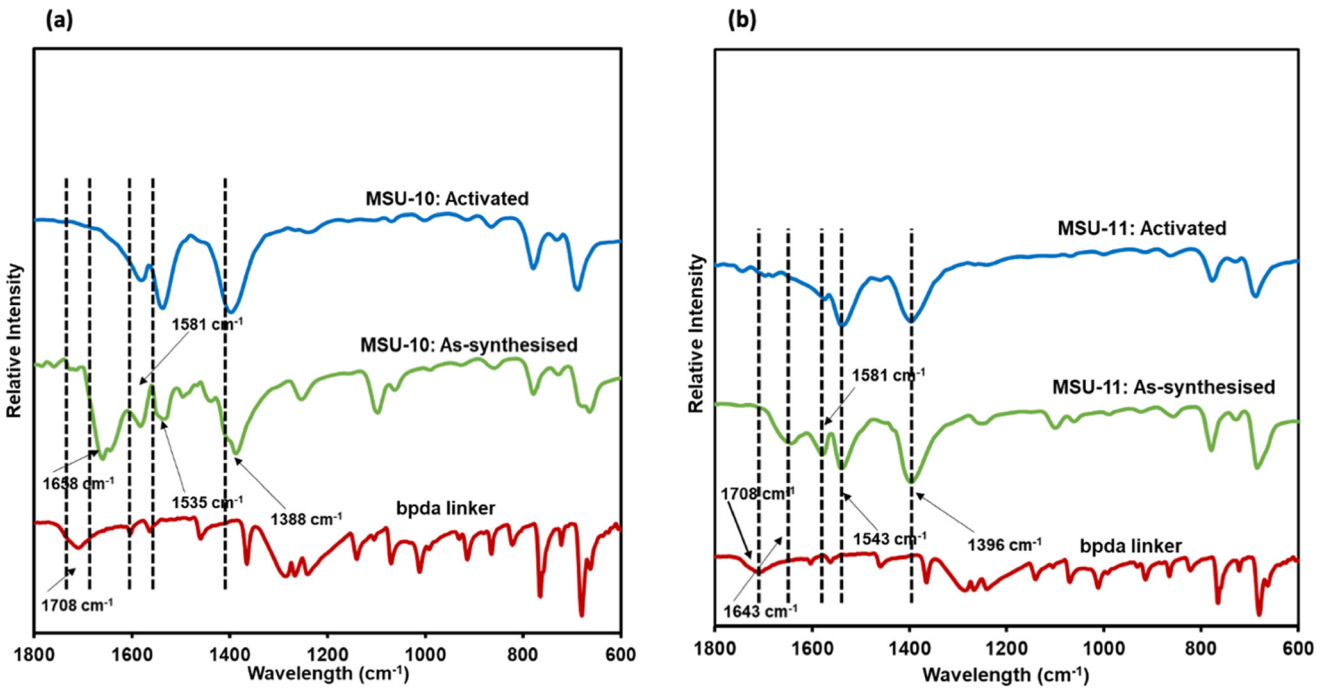

Fig. 7 FTIR studies of (a) MSU-10 and (b) MSU-11.

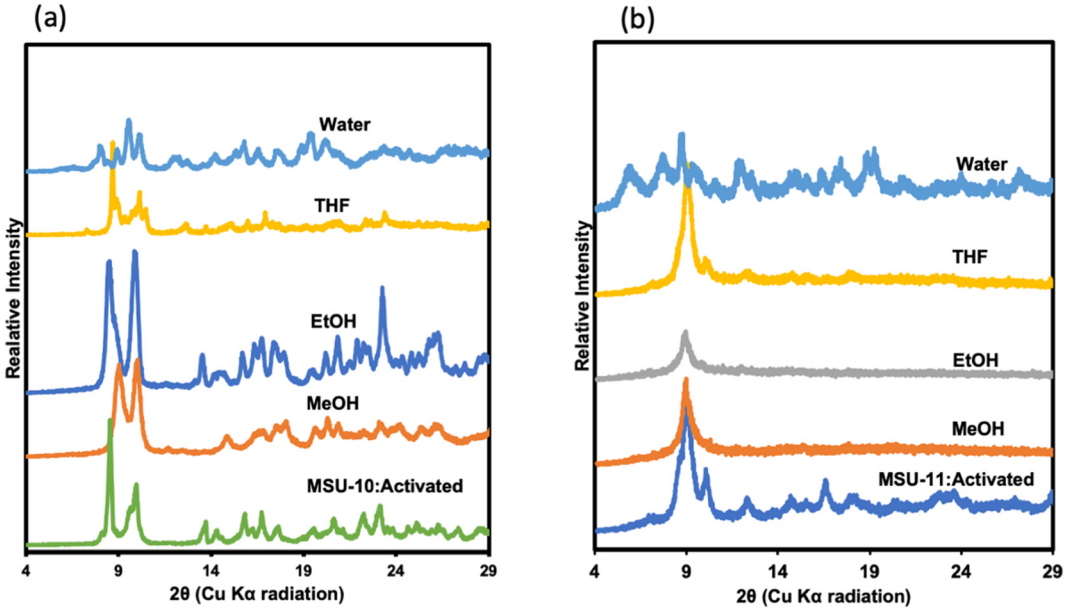

Fig. 8 PXRD patterns of a) MSU-10 and b) MSU-11 in different chemical environments.

Gas sorption studies

The expected microporosity, could be detected by gas sorption, see Fig. S3.† We note this could be due to framework collapse, we do see some amorphisation after activation, but also due to the structures as such. MSU-11, though having fairly large calculated porosity, has channels in shape of narrow slits with openings of only around 2.6 Å.

Conclusions

In our effort do design and synthesize new MOFs that can be used for carbon dioxide capture and conversion,[23] two novel MOFs of $[La(bpdc)_{3/2}(dmf)_2]\cdot(dmf)(H_2O)$, MSU-10 and $[La(bpdc)_{3/2}(H_2O)_2(dmf)]\cdot dmf$, MSU-11 were synthesized. The use of a modulator, 1,10-phenathroline yielded a 3D MOF, (MSU-11), with a very rare **zbj** topology while the 2D network MSU-10 was formed without modulator. The rod-SBUs in MSU-11 are linked by single and double linker connections. Network topology analysis led us to identify MOF-80 with a different linker and metal ion, Tb(III), as a very similar structure, albeit with significantly different unit cell parameters. We note MOF-80 was prepared without modulator but with a different solvent mixture, underlining the complexity of MOF synthesis. Chemical stability studies revealed that both frameworks undergo some phase transitions upon soaking in protic solvents.

Author contributions

Johannes Hungwe; methodology, investigation, writing – original draft preparation, Piwai Tshuma; supervision, conceptualization, resources, writing – reviewing and editing. Maureen Gumbo; investigation and methodology, Francoise M. Amombo Noa; methodology, investigation, reviewing and editing, Lars Öhrström; software, investigation, reviewing and editing, Gift Mehlana; supervision, conceptualization, investigation, methodology, software, resources, writing – reviewing and editing.

Conflicts of interest

The authors declare no conflict of interest.

Acknowledgements

Funding for this project was provided by The Royal Society through the Future Leaders African Independent Research Program grant number FLR\R1\191510. The Authors would also like to thank the Swedish Research Council and the Midlands State University Research Board for financial support. The authors would like to thank Ocean Cheung, Uppsala University, for the gas sorption studies and Chalmers Materials Analysis Laboratory, CMAL, and the Olle Enqvist Foundation for funding the single crystal diffractometer. We thank the Berkely Global Science Institute for providing network support.

References

1 A. K. Cheetham, C. N. R. Rao and R. K. Feller, *Chem. Commun.*, 2006, 4780.
2 C. A. Trickett, A. Helal, B. A. Al-Maythalony, Z. H. Yamani, K. E. Cordova and O. M. Yaghi, *Nat. Rev. Mater.*, 2017, **2**, 17045.
3 C. Pagis, M. Ferbinteanu, G. Rothenberg and S. Tanase, *ACS Catal.*, 2016, **6**, 6063.
4 B. Ugale, S. S. Dhankhar and C. M. Nagaraja, *Cryst. Growth Des.*, 2018, **18**, 2432.
5 H. Y. Li, Y. L. Wei, X. Y. Dong, S. Q. Zang and T. C. W. Mak, *Chem. Mater.*, 2015, **27**, 1327.

6 D. Bejan, L. G. Bahrin, S. Shova, N. L. Marangoci, Ü. Kökcam-Demir, V. Lozan and C. Janiak, *Molecules*, 2020, **25**, 3055.
7 J. Zhu, P. M. Usov, W. Xu, P. J. Celis-Salazar, S. Lin, M. C. Kessinger, C. Landaverde-Alvarado, M. Cai, A. M. May, C. Slebodnick, D. Zhu, S. D. Senanayake and A. J. Morris, *J. Am. Chem. Soc.*, 2018, **140**, 993.
8 B. Ugale, S. S. Dhankhar and C. M. Nagaraja, *Inorg. Chem.*, 2016, **55**, 9757.
9 A. Schoedel, M. Li, D. Li, M. O'Keeffe and O. M. Yaghi, *Chem. Rev.*, 2016, **116**, 12466.
10 F. M. Amombo Noa, M. Abrahamsson, E. Ahlberg, O. Cheung, C. R. Göb, C. J. McKenzie and L. Öhrström, *Chem*, 2021, **7**, 2491.
11 N. L. Rosi, J. Kim, M. Eddaoudi, B. Chen, M. O'Keeffe and O. M. Yaghi, *J. Am. Chem. Soc.*, 2005, **127**, 1504.
12 N. R. Catarineu, A. Schoedel, P. Urban, M. B. Morla, C. A. Trickett and O. M. Yaghi, *J. Am. Chem. Soc.*, 2016, **138**, 10826.
13 A. Schoedel, M. Li, D. Li, M. O'Keeffe and O. M. Yaghi, *Chem. Rev.*, 2016, **116**, 12466.
14 E. V. Alexandrov, A. V. Goltsev, R. A. Eremin and V. A. Blatov, *J. Phys. Chem. C*, 2019, **123**, 24651.
15 W. Mao, R. Huang, H. Xu, H. Wang, Y. Huang, S. Huang and J. Zhou, *Polymers*, 2022, **14**, 3826.
16 G. Mehlana, C. Wilkinson, C. T. Dzesse, G. Ramon and S. A. Bourne, *Cryst. Growth Des.*, 2017, **17**, 6445.
17 R. S. Forgan, *Chem. Sci.*, 2020, **11**, 4546.
18 F. E. Chen, T. A. Pitt, D. J. Okong'o, L. G. Wetherbee, J. J. Fuentes-Rivera and P. J. Milner, *Chem. Mater.*, 2022, **34**, 3383.
19 J. L. C. Rowsell and O. M. Yaghi, *Microporous Mesoporous Mater.*, 2004, **73**, 3.
20 J. Ha, J. H. Lee and H. R. Moon, *Inorg. Chem. Front.*, 2019, **7**, 12.
21 M. J. Kalmutzki, N. Hanikel and O. M. Yaghi, *Sci. Adv.*, 2018, **4**, 1.
22 P. Tshuma, B. C. E. Makhubela, N. Bingwa and G. Mehlana, *Inorg. Chem.*, 2020, **59**, 6717.
23 P. Tshuma, B. C. E. Makhubela, C. A. Ndamyabera, S. A. Bourne and G. Mehlana, *Front. Chem.*, 2020, **8**, 1.
24 *SAINT, version 7.60a*, Bruker AXS Inc, Madison, WI, USA, 2006.
25 *Crysalis CCD*, Oxford Diffraction Ltd, Abingdon, Oxfordshire, UK, 2005.
26 G. M. Sheldrick, *Acta Crystallogr., Sect. C: Struct. Chem.*, 2015, **71**, 3.
27 L. J. Barbour, *J. Supramol. Chem.*, 2003, **1**, 189.
28 A. A. Coelho, *TOPAS-Academic, version 4.1 (Computer software)*, Coelho Software, Brisbane, 2007.
29 G. S. Pawley, *J. Appl. Crystallogr.*, 1981, **14**, 357.
30 O. D. Friedrichs, *Systre 1.1.4beta*, 2007, **https://gavrog.sourceforge.net/**.
31 V. A. Blatov and V. Peaskov, *Acta Crystallogr., Sect. B: Struct. Sci.*, 2006,62, 457.
32 M. O. Keeffe, M. A. Peskov, S. J. Ramsden and O. M. Yaghi, *Acc. Chem. Res.*, 2008, **41**, 1782.
33 A. L. Spek, *Acta Crystallogr., Sect. D: Biol. Crystallogr.*, 2009, **65**, 148.
34 F. M. Amombo Noa, E. Svensson Grape, S. M. Brülls, O. Cheung, P. Malmberg, A. K. Inge, C. J. Mckenzie, J. Mårtensson and L. Öhrström, *J. Am. Chem. Soc.*, 2020, **142**, 9471.
35 L. Öhrstrçm, *Chem. - Eur. J.*, 2016, 1.
36 A. López-Olvera, J. Antonio Zárate, E. Martínez-Ahumada, D. Fan, M. L. Díaz-Ramírez, P. A. Sáenz-Cavazos, V. Martis, D. R. Williams, E. Sánchez-González, G. Maurin and I. A. Ibarra, *ACS Appl. Mater. Interfaces*, 2021, **13**, 39363.
37 G. Mehlana, S. A. Bourne, G. Ramon and L. Öhrström, *Cryst. Growth Des.*, 2013, **13**, 633.

